Evaluation of Existing Masonry Structures under Multiple Extreme Impacts

PETRUS Cristian [a], MARIC Dario [b], THOMAIDIS Ioannis [c], THOMAIDIS Ioannis – Prodromos [c], PIOMBO Silvia [d], SCAGLIOTTI Giulia [e], DIMITRENKO Evgeniy [f], TIRADO Rodolfo Javier [g], KAHSAY HAGOS Simon [h]

[a] *Politehnica University of Timisoara, Faculty of Civil Engineering, Romania*

[b] *University Josip Juraj Strossmayer Osijek, Faculty of Civil Engineering, Croatia*

[c] *Aristotle University of Thessaloniki, Faculty of Civil Engineering, Greece*

[d] *Universita degli Studi di Genova, Scuola Politecnica, Department of Civil Engineering, Italy*

[e] *Universita degli Studi di Pavia, Faculty of Civil Engineering and Architecture, Italy*

[f] *National Aviation University, Institute of Airports, Department of Computer Technologies in Constructions, Kiev, Ukraine*

[g] *Universidad Industrial de Santander, Faculty of Civil Engineering, Bucaramanga, Colombia*

[h] *Bauhaus-Universität Weimar, Faculty of Civil Engineering, Germany*

ABRAHAMCZYK Lars, SCHWARZ Jochen

Earthquake Damage Analysis Center, Bauhaus-University Weimar, Germany

Abstract

In close collaboration with local partners, Earthquake Damage Analysis Centre (EDAC) of Bauhaus University Weimar initiated a Turkish-German joint research project on Seismic Risk Assessment and Mitigation in the Antakya-Maraş-Region (SERAMAR). In this context, the instrumental investigation of buildings being representative for the study area becomes an essential part of the project to calibrate the models and to predict reliable capacity curves as well as scenario-dependent damage pattern or failure modes. A number of masonry buildings have been chosen and could be temporarily and permanently equipped with modern Seismic Building Monitoring Systems (BMS).

In this paper, one of the temporarily instrumented masonry buildings will be investigated in detail to evaluate the dynamic response and horizontal load bearing capacity under seismic action. The available response measurements are elaborated and the real response characteristic of the study object determined as input parameters for the model calibration and validation. The capacity of the study building is determined for different model assumptions to consider the model uncertainties in the damage prognosis. Therefore, a 3D numerical model is created using the computer software SAP2000, whereas the masonry walls are represented by piers and spandrels following the equivalent frame approach. The nonlinear behavior of the elements is described by non-linear hinges following a set of different available formulas and approaches.

Finally, an experimental testing on small scale approximation of the real structure could be conducted in part of the project. The Experiment pointed out the vulnerable character of the structure when it is subjected to an earthquake after earthquake scenario.

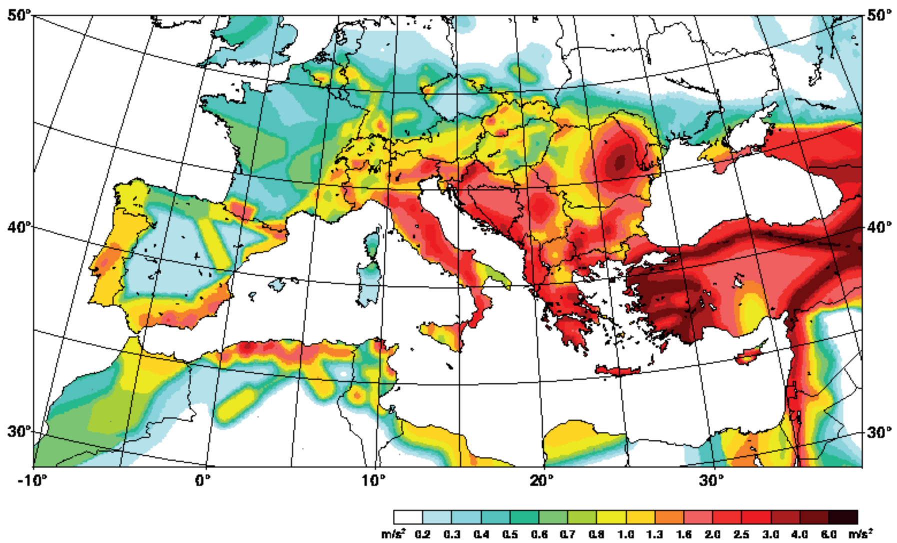

Figure 1. Seismic zonation map of Europe [1]

Introduction

History as well as recent recordings has shown us that earthquakes impact our daily lives in such a way that the engineers and architects try to build a risk free and healthy environment for the community. Due to the variable nature of ground motion, such a task is rarely achieved. Earthquakes occur all over the world and are a result of a sudden release of energy from the Earth's crust. This affects all surrounding regions in a manner influenced by soil factors, wave propagation and intensity of the seismic wave. Almost half of the European continent is affected by seismic activity, as it can be seen in Figure 1.

Earthquakes are a present hazard which were also mentioned in ancient times by historians and scribes, which recorded in writing the damages and effects of the extreme events in a subjective manner. In present times, more objective technologies and techniques are used to evaluate the magnitude of an earthquake. Since all of Turkey is vulnerable to seismic activities, in Figure 2 it can be observed a history of the seismic events which occurred on the current territory of the country.

Recent events, such as the one from the Van province from 2011 having a magnitude of 7.1 on the Richter scale, reminded us of the destructive force of the ground motion, as it can be seen in Figure 3.

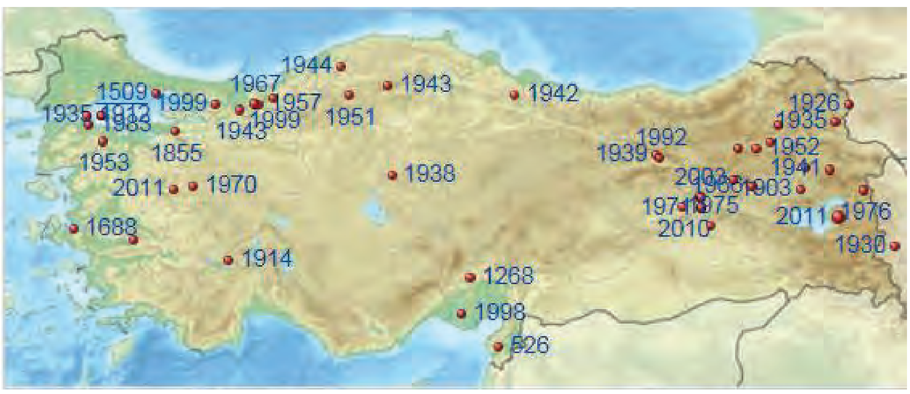

Figure 2. History of earthquakes in Turkey

[https://en.wikipedia.org/wiki/List_of_earthquakes_in_Turkey]

Figure 3. Damages of buildings after the Van earthquake, 2011

[http://www.eqclearinghouse.org/2011-10-23-eastern-turkey/2011/10/31/photos-of-earthquake-damage/, photos from I. Bedirhanoglu]

Case study

The proposed structure to be analysed is a real structure from the city of Antakya, situated in the South-eastern part of Turkey near the East Anatolian seismic fault [2 - 4]. The building is made of masonry and has 4 stories and a length of 22.7m by 11.2m with a storey height of 2.8m. The initial plans of the building showed 4 storeys on one side and 3 storeys on the other. Due to recent interventions, there was constructed an additional level on one side of the building, and modified the sensitivity to torsional effects. From the provided architecture plans, an area of 14.53m^2 was observed for the longitudinal walls and 9.52m^2 for the transversal walls. An overview of the building and the floor plan can be taken from Figure 4.

Figure 4. View of the existing building and floor plan (Source: EDAC)

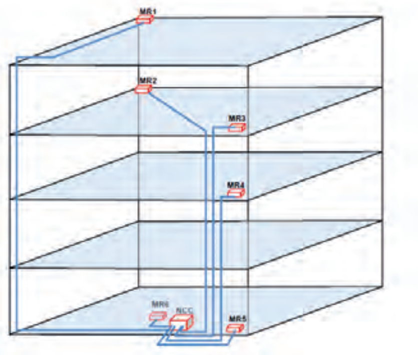

Figure 5. Location of the sensors

Dynamic characteristics of the existing structure

In order to calibrate the finite element model of the building to correspond with the real behavior of the existing building, six sensors were placed on different floors recording and transmitting ambient noise data. The sensors were recording the micro-vibrations in terms of velocity (mm/sec) in three axes (X, Y, Z).

Each sensor was active for around 25 minutes and the data was separated into 25 files of 1 minute each. The sampling rate of the sensors was 100 Hz. The divided files were subsequently combined into one master file for each axis, showing the velocity time history of each sensor due to ambient noise. In order to correct the error of the sensors, which has displaced the neutral axis from zero, baseline correction was applied by subtracting the mean value from each measurement.

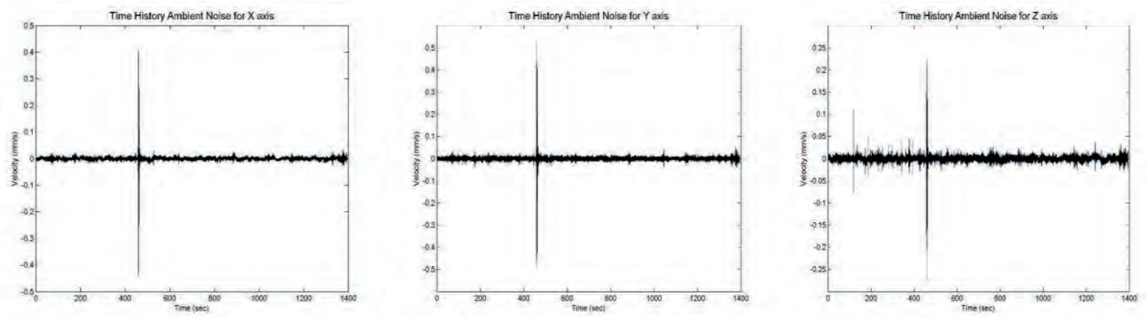

Figure 6. Time histories of sensor MR1 for axes X, Y, Z

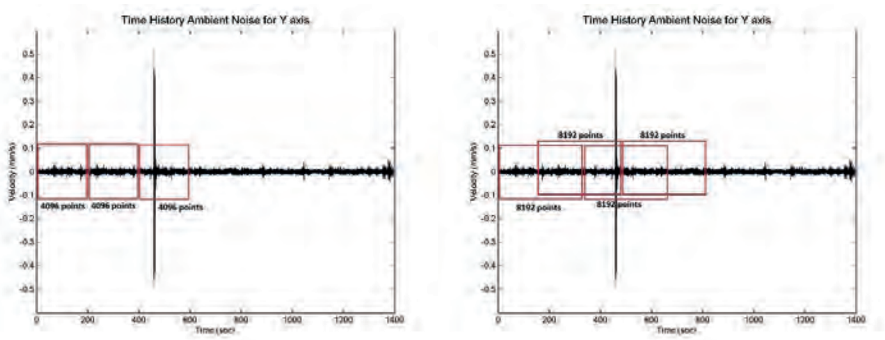

Figure 7. Parallel segments (4096 points) and overlapping segments (8192 points)

The purpose of this procedure is to identify the dynamic characteristics of the existing structure, explicitly the Eigen frequencies. To achieve this, it is required to translate the data from the time domain to the frequency domain by using the Fast Fourier Transformation and produce Fourier Spectrums. With a view to accomplish a better accuracy, the segmentation of the time histories was determined to by using two different methods. In the first one, it was decided to pick in succession segments of 4096 points each, while in the second one overlapping segments of 8192 points each.

The procedure was implemented to every segment of each axis of all sensors. In total, for each time history, there were 34 segments for the first method and 33 for the second one and the Fourier Spectrums were calculated for all of them. Consequently, it was calculated the mean and the standard deviation of all the processed data for every sensor. Comparing the diagrams between the two different methods, it is concluded that there is high convergence of the amplified frequencies.

Although it is already possible to reach a conclusion for the frequencies from the previous diagrams, in order to pinpoint the Eigen frequencies of the existing structure, it is essential to exclude any outside influences (moving cars, footsteps etc.) from the Fourier Spectrums. This is feasible by calculating the Spectrum ratios between the sensors which are located to the top floors and those on the base. The most representative result is given by the ratio of the top floor (4th) to the base of the building (MR1/MR6) but the same result was achieved by other ratios as well (MR2/MR6). The results from the ratios of sensors MR3 and MR4 were discarded because of the low amplification and the difficulty to determine the Eigen frequencies.

The peak amplification for both methods is concentrated around the frequencies 6.15 Hz for the X axis and 4.67 Hz for the Y axis.

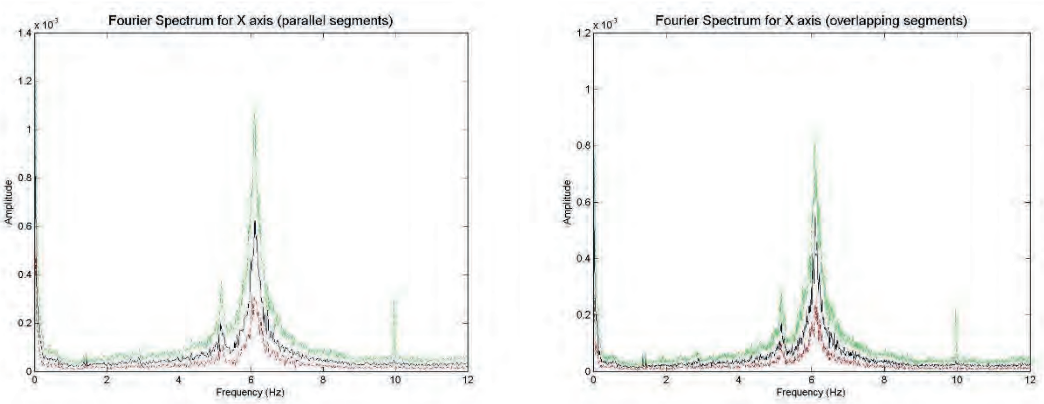

Figure 8. Fourier Spectrums of 16th percentile, mean and 84th percentile for the two methods

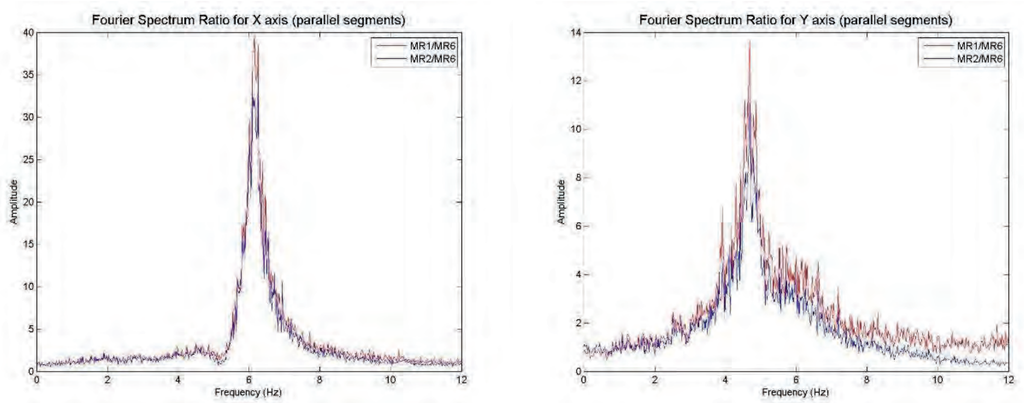

Figure 9. Fourier spectrum ratios between MR1 to MR6 for X and Y axis

Table 1. Measured Eigen frequencies and Periods of the structure

	X axis	Y axis
Frequency (Hz)	6,15	4,67
Period (sec)	0,163	0,214

Equivalent Frame Model

Simplified Analysis Method (SAM), developed since 1996 by *Magenes and Calvi*, and then modified by *Magenes and Della Fontana*. The SAM, considers that spandrel as deformable; furthermore it can move horizontally and can rotate. In the SAM, the wall is schematized with an equivalent frame composed by: column elements representing the piers; beam elements representing the spandrels; rigid offsets describing the joint panel. The joint is considered infinitely rigid because generally (but not always) this area is not cracked.

Both the pier and the spandrel have an elastic-plastic behaviour with a deformation limit; in particular, the element is considered elastic until it reaches the threshold of a failure criterion (rocking, diagonal shear and sliding shear for pier; rocking and shear for spandrel); once the threshold is exceeded, a plastic hinge is activated. The nonlinearity of the material is taken into account through the use of plastic hinges. Three types of plastic hinges are used: shear hinges (V type), bending hinges (M type) and rocking hinges (PM type).

- For the piers are used V and PM hinges. The V hinges are placed in the middle of the deformable part of the piers, the PM hinges at the end of it.
- For the spandrels are used V hinges in the middle of the spandrel, and M hinges at the end of it.

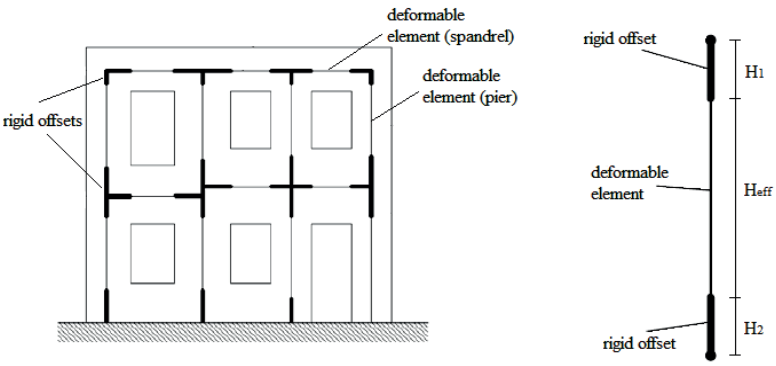

Figure 10. Equivalent frame wall using rigid offsets

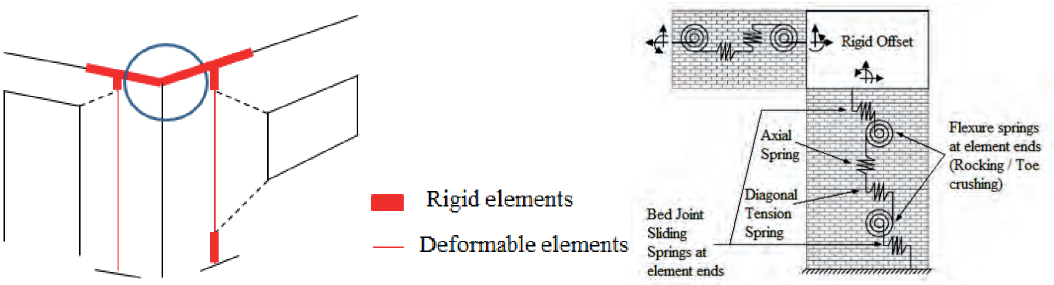

Figure 11. Rigid Offset (stiff behaviour) and Deformable Element (elastic to plastic behaviour)

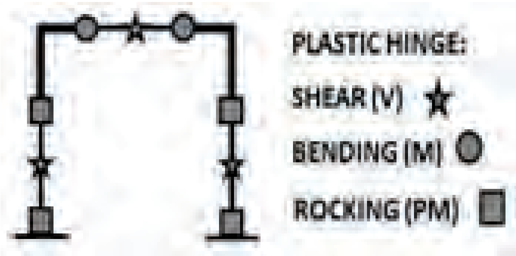

Figure 12. Location and type of plastic hinges

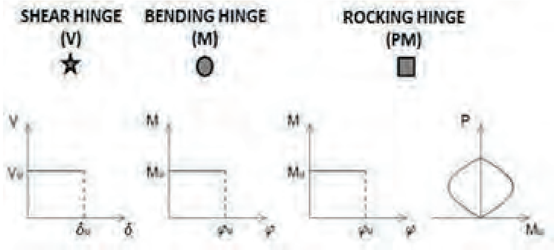

Figure 13. Behaviour of the different plastic hinges

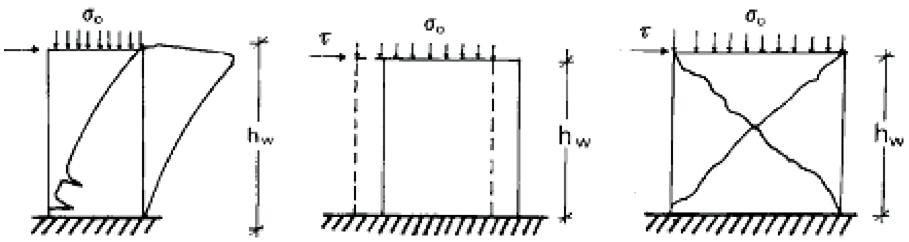

Figure 14. In-plane failure modes of masonry walls a) rocking; b) sliding; c) diagonal cracking

The behaviour that has been assigned to the various hinges is shown in Figure 13: the V hinges take into account the relationship between the ultimate displacement of the panel δ_u and the limit shear V_u, and the M hinges between the moment M_u and ultimate rotation φ_u; on the other hand, the PM hinges consider the interaction between the normal stress P and the ultimate moment M_u.

Proposal of different nonlinear hinge definitions

According to *Pasticier et al.* [5] the strength in terms of ultimate moment M_u is defined by Equation (1). As far as the shear strength is concerned, according to the experimental test outcomes [7], authors of [1] decided to consider two strength criteria. The first criterion (Eq. 2) is recommended in [6] for existing buildings.

This criterion, which refers to shear failure with diagonal cracking, was originally proposed by *Turnsek and Cacovic* [8] and later modified by *Turnsek and Sheppard* [9]. The second criterion (Eq. 3) refers to shear failure with sliding and is recommended in [6] for new buildings. Although formulated differently, such a criterion is also recommended by the Eurocode 8 [10].

$$M_u = \frac{\sigma_0 D^2 t}{2}\left(1 - \frac{\sigma_0}{kf_d}\right) \tag{1}$$

$$V_u^f = \frac{1.5 f_{v0d} Dt}{\xi}\sqrt{1 + \frac{\sigma_0}{1.5 f_{v0d}}} \tag{2}$$

$$V_u^s = \frac{\frac{3}{2} f_{v0d} + \mu \frac{\sigma_0}{\gamma_m}}{1 + \frac{3H_0}{D\sigma_0} f_{v0d}} Dt \tag{3}$$

where σ_0 is the mean vertical stress, D the pier width, t the pier thickness, k the coefficient taking into account the vertical stress distribution at the compressed toe, f_d the design compression strength, f_{v0d} the design shear strength with no axial force; μ (friction coefficient) = 0.4, the coefficient related to the pier geometrical ratio, H_0 the effective pier height, and γ_m the safety factor.

For the rocking hinges the strength is given by Equation (1), and the ultimate rotation ϕ_u corresponds to an ultimate lateral deflection δ_u equal to 0.8% of the deformable height of the pier, minus the elastic lateral deflection, as recommended in [6]. For the shear hinge, the strength is given by the minimum value resulting from Equations (2) and (3). The ultimate shear displacement δ_u was assumed to be equal to 0.4% of the deformable height of the pier, minus the elastic lateral deflection, as recommended in [6].

As far as the modelling of the spandrel beams is concerned, assuming the presence of a lintel properly restrained at both supports, only one 'shear hinge' was introduced at mid-span (Figure 3a), with the shear strength V_u given by

$$V_u = htf_{\upsilon 0d} \tag{4}$$

where h is the spandrel depth, t the spandrel thickness, and f_{v0d} the design shear strength with no axial force.

According to *Bal et al.* [11] three different types of failure modes have been considered for the piers like in work [5]: flexural (rocking) (see Eq. 5), diagonal shear (see Eq. 6) and sliding shear (see Eq. 7).

$$M_u = \frac{pD^2t}{2}\left(1 - \frac{p}{kf_u}\right) \tag{5}$$

$$V_y^d = \frac{f_{tu}Dt}{b}\sqrt{1 + \frac{p}{f_{tu}}} \tag{6}$$

$$V_y^s = \frac{f_{tu} + \mu\dfrac{p}{\gamma_m}}{1 + \dfrac{2H_0}{Dp}f_{tu}} \tag{7}$$

where f_{tu} represents the conventional tensile strength of masonry (not the tensile strength of the bed joints), b is a parameter which is assumed to be dependent on the *H/D* aspect ratio of the pier (like ξ at *Pasticier et al.* [5]), p is the mean vertical stress on the pier, f_u is the compressive strength of masonry.

Bal et al. [11] propose two failure modes for the spandrels: flexural (see Eq. 8) and shear. The ultimate shear capacity is given as $V_u = f_{v0d}ht$ as well as *Pasticier et al.* [5].

$$M_u = \frac{H_p h}{2}\left(1 - \frac{H_p}{kf_{hd}ht}\right) \tag{8}$$

where H_p is the minimum of the horizontal shear resistance of the element or the value $0.4f_{hd}ht$, f_{hd} is the compressive strength of the masonry in the horizontal direction in plan of the wall.

According to *Diogo et al.* [12] Equations (9), (10), (11) define the failure modes for piers:

$$M_u = \frac{\sigma_0 D^2 t}{2}\left(1 - \frac{\sigma_0}{kf_d}\right) \text{ - rocking} \tag{9}$$

$$V_{rd} = \frac{1.5 C_u Dt}{\xi}\sqrt{1 + \frac{\sigma_0}{1.5 \cdot C_u}} \text{ - diagonal cracking} \tag{10}$$

$$V_{rd} = \frac{1.5 C_u + \sigma_0 \tan\varphi}{1 + \frac{3 \cdot H_0}{\sigma_0 D} C_u} Dt \text{ - sliding} \tag{11}$$

where, C_u is the cohesion; φ is the friction internal angle; H_0 is the distance from zero moment section to control section.

Diogo et al. [12] argue that in spandrels the rupture is usually due to shear and its resistance is often regarded as being owed to material cohesion (see Eq. 12).

$$V_{rd} = htC_u \tag{12}$$

According to *Bucchi et al.* [13] following equations (13), (14), (15) define the failure modes for piers:

$$M_u = \frac{\sigma_0 D^2 t}{2}\left(1 - \frac{\sigma_0}{kf_d}\right) \text{ - rocking} \tag{13}$$

$$V_{uf} = \frac{f_{td} Dt}{\xi}\sqrt{1 + \frac{\sigma_0}{f_{td}}} \text{ - diagonal cracking} \tag{14}$$

$$V_{us} = l' t f_{vd} \text{ - sliding} \tag{15}$$

where f_{td} – diagonal shear strength, f_{vd} - sliding shear strength in absence of normal stress, f_{hd} - compression strength in horizontal direction; l' – length of compressed part of pier.

For definition of spandrels strength criteria authors of [13] use Equations (16), (17):

$$M_u = \frac{H_p h}{2}\left(1 - \frac{H_p}{kf_{hd} ht}\right) \text{ - rocking} \tag{16}$$

$$V_{rd} = htf_{vd} \text{ - sliding} \tag{17}$$

And finally, according to *Lagomarsino et al.* [14] strength criteria of piers are defining by Equations (18), (19), (20):

$$M_u = \frac{N \cdot l}{2}\left(1 - \frac{N}{kf_m lt}\right) \text{ - rocking} \tag{18}$$

$$V_{uf} = \frac{\tau_0 Dt}{\xi}\sqrt{1 + \frac{N}{1.5 \cdot \tau_0 lt}} \text{ - diagonal cracking} \tag{19}$$

$$V_{us} = l' t C_u + \mu N \text{ - sliding} \tag{20}$$

where N – axial load; f_m – compression strength; τ_0 – diagonal shear strength; C_u – cohesion; f_{hd} – compression strength in horizontal direction.

For spandrels authors of [14] consider 2 strength criteria – rocking and sliding (see Eq. 21, 22):

$$M_u = \frac{H_p h}{2}\left(1 - \frac{H_p}{kf_{hd} ht}\right) \text{ - rocking} \tag{21}$$

$$V_{rd} = htC_u \text{ - sliding} \tag{22}$$

As we can see from the above works, there are substantial differences in the formulas of the strength criteria of nonlinear elements frame hinges simulating the work of masonry walls under seismic load. A comparison of the hinge definition results obtained by previous researchers is presented in the following figures.

Material and mechanical parameters involved in hinge definitions leads to under or over prediction of the actual strength of the structure. It is difficult to single out an accurate hinge definition without model validation, due to strong variability in results.

Numerical modelling

According to the provided architecture plans, the equivalent frame was created in SAP2000®. A new model was set by using the *3D Frames* command. Joint restraints were assigned at the base of the building in order to constrain the grades of freedom (rotation and translation in the three directions). The material characteristics used for masonry were: density of 11 kg/m^3, modulus of elasticity 3600 N/mm^2 and Poisson's ratio of 0.25. For each frame, in X and Y direction, there were assigned sections for the piers, spandrels and also there was defined the rigid offsets in order to obtain the equivalent frame.

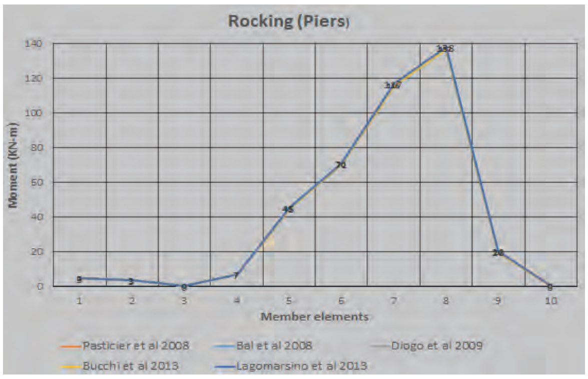

Figure 15. Rocking plots for piers

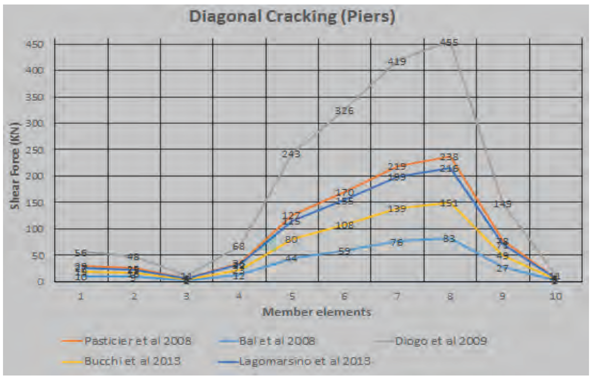

Figure 16. Diagonal plots for shear in piers

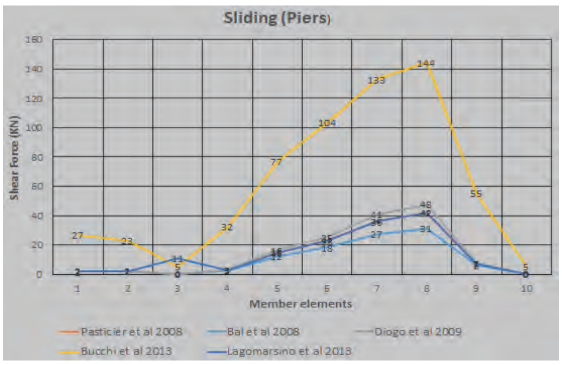

Figure 17. Sliding plots for shear in piers

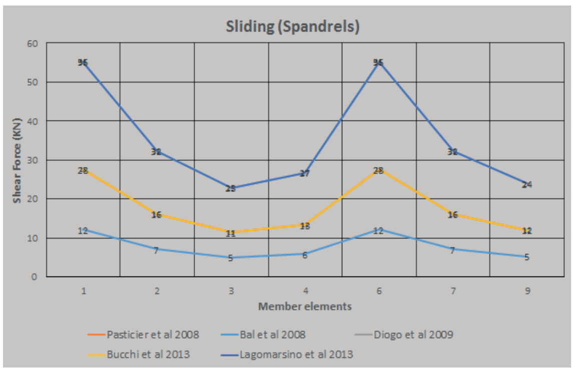

Figure 18. Sliding plots for shear in spandrels

The dead load for the slabs was considered 6 kN/m^2 and the live load 2 kN/m^2 in accordance to Eurocode 0. For the mass source, the dead load was taken with a coefficient of 1.0 and the live load with 0.3, according to Eurocode 8: The behaviour of the plastic hinges were defined in terms of moments-rotations and forces-displacements and the following four criteria were chosen: Pasticier, Bucchi, Bal and Lagomarsino. Different hinge parameters were set for all the piers and spandrels for each one of the previous four criteria. In order to simplify the model, same parameters were assigned to the groups of similar piers and spandrels. These parameters were calculated at the average of the actual values of all elements of each group. The following acceptance limits were fixed at 100%, 60% and 30% of the rotation capacity for collapse prevention, life safety and immediate occupancy. For this model, a linear variation of the rotation of the plastic hinge was implemented. Using modal analysis, the period of vibration of the structure was verified and, there were obtained similar results to the period measured by the sensors, both in X and Y direction.

Nonlinear pushover analysis

In order to obtain the pushover curves, two load distributions having linear and constant variation were used, for both X and Y directions. The plastic hinge positions can be observed in the following figure, in which the collapse state hinge is shown in red.

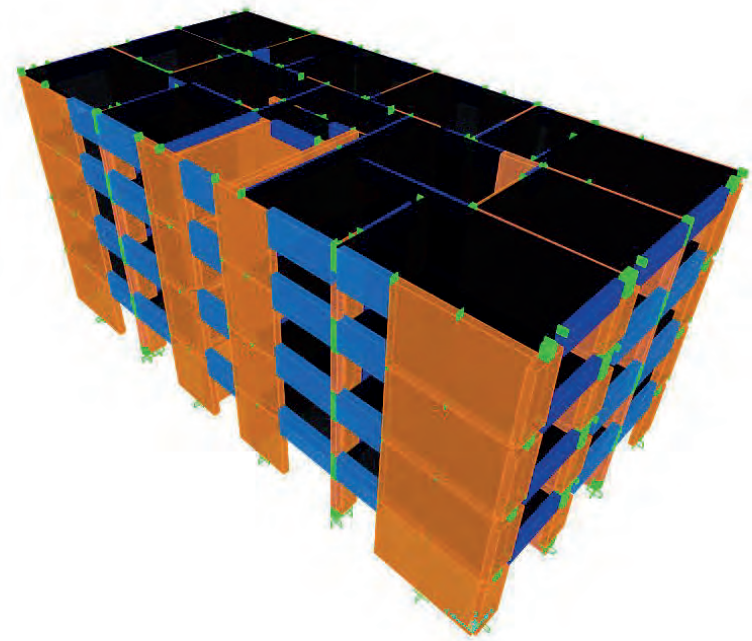

Figure 19. Equivalent 3D frame model in SAP2000

Table 2. Eigen frequencies and Periods of the structure.

	Measured		Calculated	
	Frequency [Hz]	Period [sec]	Frequency SAP2000 [Hz]	Period SAP2000 [sec]
X axis	6,15	0,16	6,81	0,14
Y axis	4,67	0,21	8,34	0,13

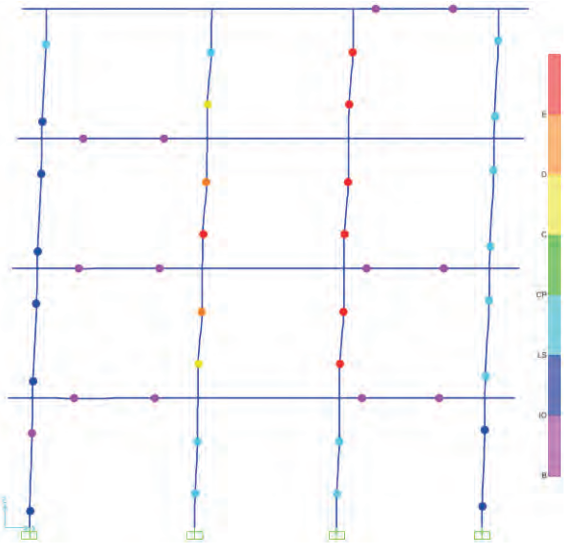

Figure 20. Image of hinge collapsing

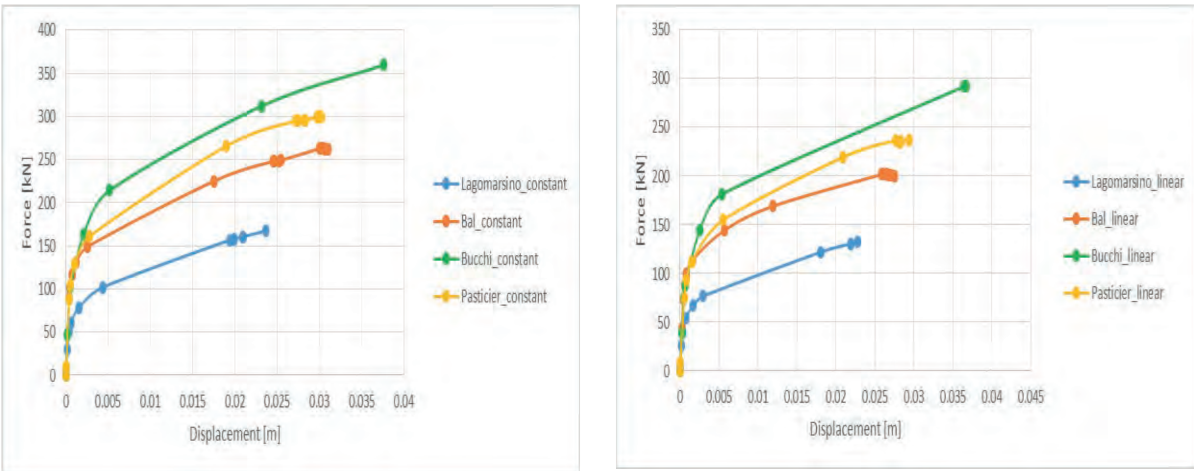

Figure 21. Pushover curves comparison for costant and linear load, X direction

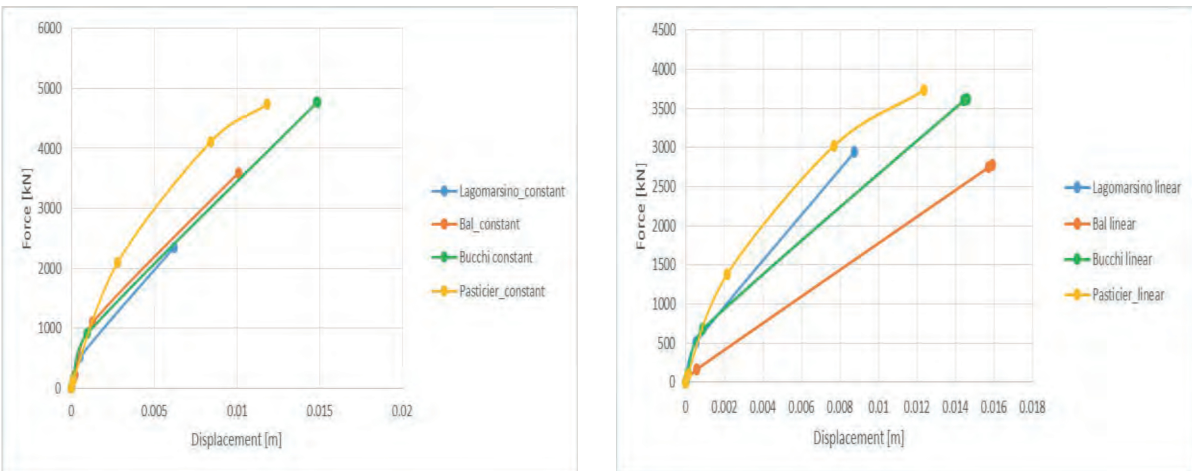

Figure 22. Pushover curves comparison for costant and linear load, Y direction

The values from the pushover curves for the four criteria of plastic hinge definitions are presented in Figures 21 and 22 for each loading type (constant and linear).

From the presented graphs it can be observed that the structure has more resistance on Y transversal direction than on longitudinal X direction.

In addition to pushover curves, there was also calculated the perfomance point for the structure, which represents the state of maximum inelastic capacity of the structure, found by crossing the point of the capacity spectrum and demand spectrum for a given damping ratio. This point was evaluated at a displacement of 1.2cm at a base shear force of 125kN.

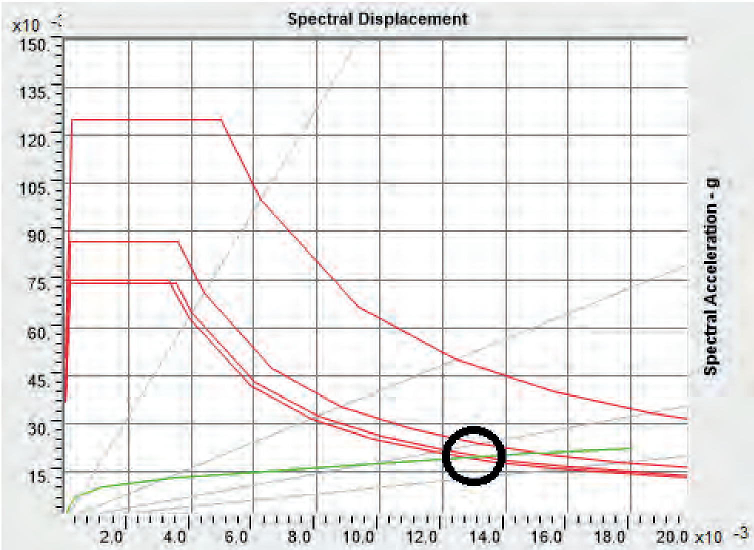

Figure 23. Performance point of the structure

Experimental Testing

There was constructed an experimental model of the building, at a scale of 1:50, which was tested on a shaking table at Bauhaus University from Weimar. The model was built using brick-like elements and wooden pieces in order to simulate the reinforced concrete slabs. This structure was used in order to validate the analytical reasoning of the building model.

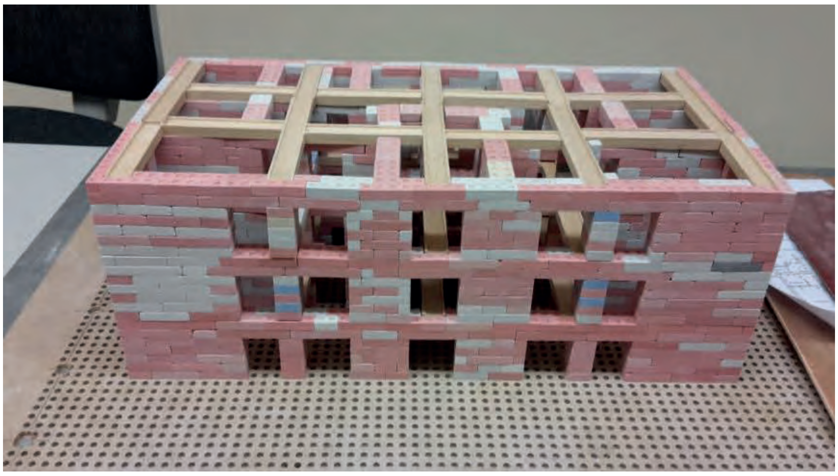

Figure 24. Building model, scale 1:50

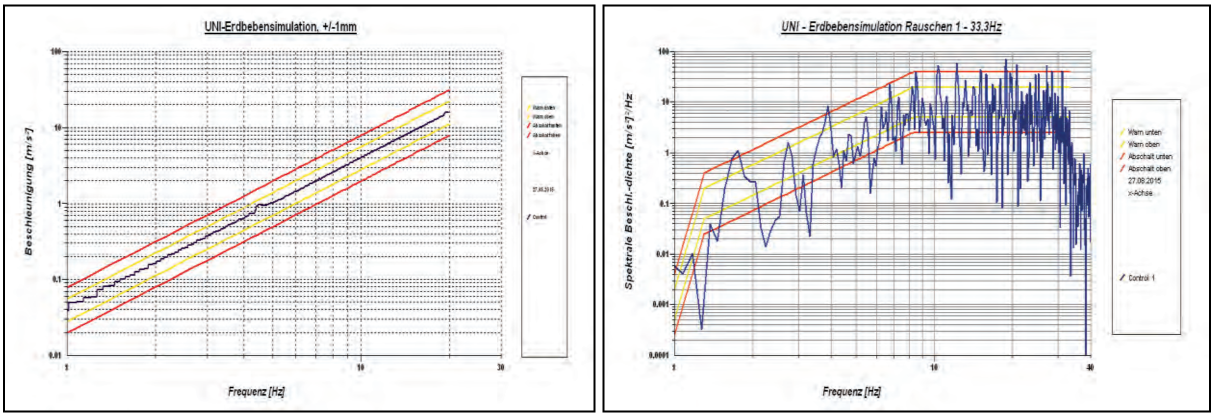

Figure 25. Simulation of seismic loading a) pre-shock; b) main shock

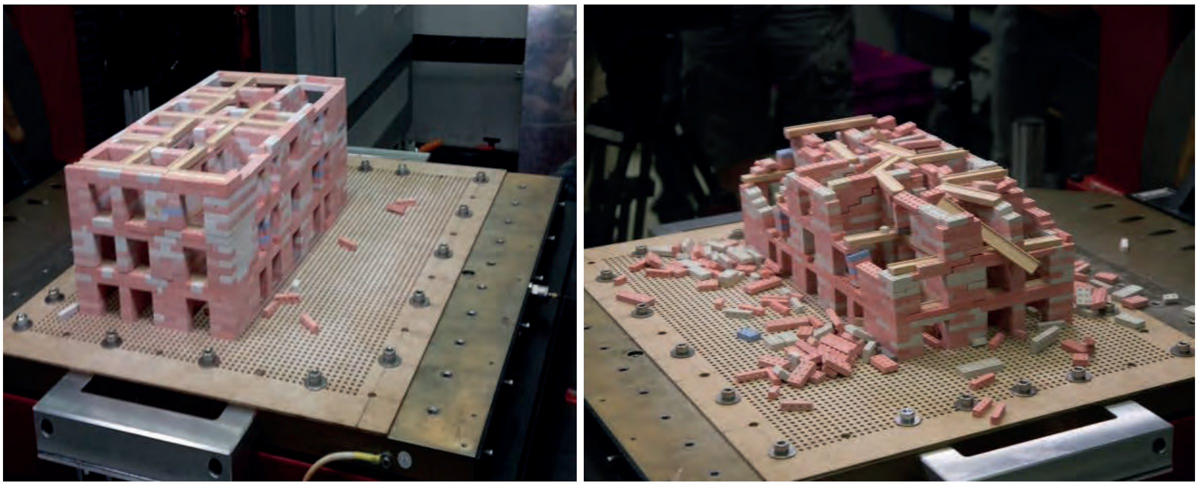

Figure 26. Consequences of seismic loading a) before; b) after main shock

The structure has been tested by a simulation of two real earthquake with different intensities. The first one (pre-shock) produced only a few damages on the top part of the model, while the second one (main-shock), characterized by a frequency of 33.3 Hz produced the collapse of the entire structure.

Conclusions

Extreme events, such as earthquakes, influence our daily lives and the way in which we build secure buildings. There has been performed a 3D nonlinear analysis on a model of an existing building from Turkey. Several proposals for the hinge definitions were studied, each having a similar approach but with different results. Pushover analysis confirms the importance of hinge definitions in order to obtain reliable results. Further investigations must be carried out in order to obtain accurate results in the nonlinear domain of masonry structures. Small scale experimental testing revealed that it is important to consider the earthquake-after-earthquake scenario in the current design and construction trends.

References

[1] Grünthal, G., Bosse, Ch., Sellami, S., Mayer-Rosa, D., Giardini, D. (1999): Compilation of the GSHAP regional seismic hazard for Europe, Africa and the Middle East. *Annals of Geophysics*, **Vol. 42, No. 6.**

[2] Abrahamczyk, L., Schwarz, J., Langhammer, T., Genes, M.C., Bikce, M., Kacin, S. and Gülkan, P. (2013): Seismic Risk Assessment and Mitigation in the Antakya-Maras Region (SERAMAR): Empirical Studies on the basis of EMS-98. *Earthquake Spectra* **Vol. 29 (3)**, 683-704.

[3] Abrahamczyk, L., Schwarz, J., Langhammer, T., Genes, M.C., Bikçe, M., Kaçin, S., Yakut, A., Erberik, A.M., Gülkan, P. (2012): Empirical and Analytical Vulnerability Assessment of the Masonry Building Stock in Antakya (Hatay/ Turkey). In Proceedings *15th World Conference Earthquake Engineering*, Lisboa, Paper 1081.

[4] Genes, M.C., Erberik, A.M., Abrahamczyk, L., Gülkan, P., Bikçe, M., Kaçin, S., Yakut, A., Schwarz, J. (2012): Vulnerability assessment of two instrumented masonry buildings in Antakya (Hatay, Turkey). In Proceedings: *10th International Congress on Advances in Civil Engineering ACE2012*, Middle East Technical University, Cultural and Convention Center, Ankara Turkey, 17-19 October 2012, Paper 1019.

[5] Pasticier, L., Amadio, C., Fragiacomo, M. (2008): Non-linear seismic analysis and vulnerability evaluation of a masonry building by means of the SAP2000 V.10 code. *Earthquake Engineering and Structural Dynamics*: **Vol. 37**: 467–485.

[6] Decree of the cabinet president No. 3274. Annex 2: Provisions for design, seismic evaluation and retrofit of buildings. Appendix No. 72 to The Italian Official Gazette, vol. 105, 20 March 2003 (in Italian).

[7] Magenes, G., Calvi, GM. (1997): In-plane seismic response of brick masonry walls. *Earthquake Engineering and Structural Dynamics*, Vol. 26(11):1091–1112.

[8] Turnsek, V., Cacovic, F. (1971): Some experimental results on the strength of brick masonry walls. Proceedings: *2nd International Brick Masonry Conference*, Stoke-on-Trent, 149–156.

[9] Turnsek, V., Sheppard, P. (1980): The shear and flexural resistance of masonry walls. Proceedings: *International Research Conference on Earthquake Engineering*, Skopje, 517–573.

[10] CEN. Eurocode 8 (2004): Design of Structures for Earthquake Resistance. Part 3: Assessment and Retrofitting of Buildings. DRAFT No. 7. Stage 49. June 2004.

[11] Bal, I.E., Crowley, H., Pinho, R. (2008): Displacement based earthquake loss assessment of Turkish masonry structures. Proceedings: *14th World Conference on Earthquake Engineering*, Beijing, China.

[12] Diogo, F. (2009): Nonlinear seismic analysis of ancient buildings – structural characterization for successful seismic retrofit. *Master Thesis*. Department of Civil Engineering. Universidade Technica de Lisboa.

[13] Bucchi, F., Arangio, S., Bontempi, F. (2013): Seismic assessment of an historical masonry building using nonlinear static analysis. Proceedings: *14th International Conference on Civil Engineering*, Scotland.

[14] Lagomarsino, S., Penna, A., Galasco, A., Cattari, S. (2013): TREMURI program: An equivalent frame model for the nonlinear seismic analysis of masonry buildings. *Engineering Structures*, **Vol. 56**, pp. 87 – 99.